Springer

KSME

Journal of Mechanical Science and Technology 25 (5) (2011) 1351~1360

www.springerlink.com/content/1738-494x
DOI 10.1007/s12206-011-0311-5

Influence of blade-tower interaction in upwind-type horizontal axis wind turbines on aerodynamics †

Hogeon Kim[1], Seungmin Lee[1] and Soogab Lee[2,*]

[1]*School of Mechanical and Aerospace Engineering, Seoul National University, Seoul, 151-742, Korea*
[2]*Institute of Advanced Aerospace Technology, School of Mechanical and Aerospace Engineering, Seoul National University, Seoul, 151-742, Korea*

(Manuscript Received July 26, 2010; Revised December 28, 2010; Accepted January 20, 2011)

Abstract

The blade-tower interaction of upwind horizontal axis wind turbines has become important to aerodynamic loading as the systems become larger. However, there are not enough studies describing these phenomena. To investigate this interaction, we performed numerical simulations for uniform, yawed, wind shear flow conditions, and various tower cases using the nonlinear vortex correction method with time-marching free wake. At 5 m/s, the change in the normal force coefficient is approximately 10% of the average. The blade root region has a larger azimuth range of the interaction and a bigger change in aerodynamic loading. The blade-tower interaction decreases as the yaw error and wind shear exponent increases. The interaction due to tower radius variations is higher than that due to tower clearance variations. With regard to stochastic load, the blade-tower interaction may affect the total fatigue load at low wind speed and in a more unstable atmospheric condition.

Keywords: Wind turbine aerodynamics; Horizontal axis wind turbine; Vortex lattice method; Blade-tower interaction

1. Introduction

The rotor blades of a horizontal axis wind turbine (HAWT) have become significantly larger, from a rotor diameter of 24 m in the 1960s to more than 120 m in the mid-2000s [2, 3]. This causes modern multi-megawatt wind power systems to experience more complex flow conditions including varying wind speed, yaw error, wind shear (ground boundary layer velocity profile), blade-tower interaction, atmospheric turbulence, dynamic inflow, and dynamic stall [4]. It is very difficult to predict the unsteady aerodynamic response of systems due to these complicated unsteady flow conditions. Although there have been many experimental and numerical studies on this subject, a thorough understanding of unsteady aerodynamics and its effect on wind turbine systems has not been realized.

Blade-tower interaction was not critical when the rotor blade was not large and elastic compared to modern multi megawatt wind turbine. However, it has become important to consider blade-tower interaction and its effects on turbine systems [5-7]. Although reduced velocity due to the tower is small compared to the downwind type, the interaction of the upwind type is a complex aerodynamic problem because a high degree of nonlinearity affects the forces on the system during the tower passage. Therefore, a prediction of aerodynamic loading must consider the blade-tower interaction.

Most studies of the blade-tower interaction are limited to downwind HAWTs. Few studies have been performed on the effect of upwind HAWT blade-tower interaction on aerodynamic loading for various wind and tower conditions. Jean-Jacques Chattot developed an unsteady vortex method that can consider tower interference of upwind turbines [7] and blade flexibility. A numerical study of fatigue load from blade-tower interaction in yawed flow and for tower distance variations was done by C. Back et al. [5] without numerical validation.

We developed an appropriate numerical tool to capture the blade-tower interaction and to perform parametric analysis for various wind and tower conditions. In this study, we used the unsteady vortex lattice method (UVLM) based on potential flow with a time-marching free wake, and the nonlinear vortex correction method (NVCM) [8] for aerodynamic analysis. Simulations of blade-tower interaction over the NREL (National Renewable Energy Laboratory) Phase VI rotor turbine are presented considering wind shear, yaw error, distance from blade to tower, and the size of the tower.

2. Nonlinear vortex correction method

Thickness and viscous effects cannot be considered by the

† This paper was recommended for publication in revised form by Associate Editor Jun Sang Park

*Corresponding author. Tel.: +82 2 880 7384, Fax.: +82 2 876 4360
E-mail address: solee@snu.ac.kr

UVLM based on potential flow. Therefore, a two-dimensional (2-D) table look-up procedure is generally used [9, 10] to consider these effects. In this procedure, the Reynolds number and the effective angles of attack are needed for the aerodynamic calculation, and these data are taken from the UVLM. However, this procedure has the problem that the UVLM evaluates the bound circulations on the lifting surface without regard to thickness and viscous effects. Thus, an incorrect effective angle of attack is evaluated, and the subsequent table look-up procedure computes incorrect aerodynamic coefficients. This problem is corrected through modification of the sectional bound vortex strength by matching the sectional lift from each method; this is the core of the NVCM approach [8].

2.1 Unsteady vortex lattice method

The UVLM is based on the potential flow condition. The governing equation of irrotational, incompressible, and inviscid flow is the Laplace equation:

$$\nabla^2 \Phi^* = 0. \tag{1}$$

To solve the Laplace equation, elementary solutions of the equation that satisfy the boundary condition are superposed. The boundary condition of a rigid body requires the normal component of velocity to the surface to be zero:

$$V_B \cdot n = 0 \tag{2}$$

$$V_B = V_\infty + V_{body} + V_{wake} - \Omega \times r \tag{3}$$

where $\boldsymbol{V_B}$ is the total velocity of the body, $\boldsymbol{V_\infty}$ is the free stream velocity, $\boldsymbol{V_{body}}$ is the induced velocity by body singularities, $\boldsymbol{V_{wake}}$ is the induced velocity by wake, $\boldsymbol{\Omega}$ is the rotational velocity, and $\boldsymbol{r}$ is the position vector on the blade.

To numerically solve Eq. (2), the blade is discretized into a set of quadrilateral vortex rings. A quadrilateral vortex and a source of constant strength are used to model the tower's surface. A linear system of equations that has unknown variables representing the circulation strength of the body panels was obtained using Eq. (2). The linear system can then be solved using lower-upper (L-U) decomposition.

There are three aerodynamic effects of blade-tower interaction. The first is the effect of induced velocity by tower on the circulation distribution, that is, $\boldsymbol{V_{body}}$ of Eq. (3) on the blade vortex panel is changed by tower (changes in the right hand side of linear equations). The second is the changes of influence coefficients due to distance between a tower and a blade (changes in the left hand side influence matrix of linear equations). The last is the effect of collision between wakes and a tower. These effects make the aerodynamic load by the blade-tower interaction.

The wake shed from the trailing edge of a rotor blade is described using a vortex ring to predict distorted wake convection. The circulation strength of the latest wake panel is equal to the strength of the trailing edge panel that was computed in the previous time step. This is the unsteady Kutta condition:

$$\Gamma_{W_t} = \Gamma_{T.E_{t-\Delta t}}. \tag{4}$$

At each time step, the free wake moves with the total convected velocity that is calculated at each vortex ring corner. Fig. 1(a) and (b) show a schematic front and side view that wake s are collided with a tower. When a line of quadrilateral vortex collides with a tower, the wake element will be declared. The dotted lines of Fig. 1(a) and (b) mean the declared line that collided with a tower. The wake element, which is declared to be in collision with the tower, is excluded from the induced velocity calculation of the wake element. Finally, using the unsteady Bernoulli equation and the pressure difference, the aerodynamic load on the blade panel can be computed.

2.2 Table look-up procedure

According to Prandtl's hypothesis, the lift of each spanwise section of a finite wing is equivalent to that of the same section of an infinite wing if the local angle of attack of the finite wing is equal to that of an infinite wing [11]. However, there are some discrepancies between 2-D airfoil data and three-dimensional (3-D) sectional data due to stall delay and tip loss. In this research, AirfoilPrep of the 3D Stall worksheet [12] was applied to the two-dimensional aerodynamic coefficients which were acquired by the wind tunnel experiments in a Reynolds number of 10^6 [17, 19] because of the difference due to stall delay. The local effective angle of attack and the Reynolds number (RE) were calculated using the UVLM. Then, the aerodynamic coefficients were obtained by interpolating from the airfoil data table according to the calculated effective angle of attack and the Reynolds number. Finally, the aerodynamic forces of each section were calculated using Eq. (5):

$$\begin{aligned} dL &= 0.5\rho V^2 C_l(\alpha, RE)dA \\ dD &= 0.5\rho V^2 C_d(\alpha, RE)dA \end{aligned} \tag{5}$$

where V is the onset velocity of the strip, dA is the strip area, C_l and C_d are aerodynamic coefficients, and α is the effective angle of attack.

2.3 Nonlinear vortex correction method

As each sectional lift from the UVLM and the table look-up procedure are matched, the sectional bound vortex strength can be corrected. This method is summarized as follows:

$$\begin{aligned} &Initial\ \ stage: if\ \ F = dL_{UVLM} - dL_{table\ \ look-up} \neq 0 \\ &then: \Gamma_{initial} \pm \Delta\Gamma \rightarrow \Gamma_{modified} \\ &Final\ stage: If\ F \rightarrow 0, then\ \ use\ \Gamma_{modified} \end{aligned}$$

where dL_{UVLM} and $dL_{table\ look\text{-}up}$ indicate sectional lift from the

UVLM and the table look-up procedure, respectively, F is the difference between these two values, and Γ indicates the bound vortex strength of the blade spanwise section. In other words, if F is not zero, F is modified to be zero using the addition or subtraction of a suitable value, which has equal value in one span wise section. The bound vortex and the angle of attack are nonlinear with respect to each other. Therefore, this process must be represented by a nonlinear system of equations:

$$\begin{aligned} F_1(\boldsymbol{x}) &= (dL_{UVLM})_1 - (dL_{table\ look\text{-}up})_1 \\ F_2(\boldsymbol{x}) &= (dL_{UVLM})_2 - (dL_{table\ look\text{-}up})_2 \\ &\vdots \\ F_n(\boldsymbol{x}) &= (dL_{UVLM})_n - (dL_{table\ look\text{-}up})_n \end{aligned} \tag{6}$$

where $x_1=\Delta\Gamma_1$, $x_n=\Delta\Gamma_n$ and $\boldsymbol{x}=(x_1, x_2, \cdots, x_n)$. Subscript n is the total number of blade spanwise sections. The vector form of Eq. (6) is given by

$$\boldsymbol{F}(\boldsymbol{x}) = 0. \tag{7}$$

Eq. (7) can be solved by applying by a sophisticated Newton-Raphson iterative method with a rapid local convergence algorithm and a globally convergent strategy [13].

3. Validation of the proposed numerical method

The rotor configuration of the NREL Phase-VI S sequence was used for the simulation of blade-tower interaction. The NREL Phase-VI turbine [16-18] has a rotor diameter of 10.508 m, and a tower with a diameter of 0.6096 m at the base and 0.4064 m at the top. The basic machine parameters are showed in Tables 1 and 2. The blade uses a S809 airfoil at all span locations.

Every calculation was performed on 20 vortex lattices along the radial directions and on two vortex lattices along the chordwise directions. The tower consists of 18 circumferential lattices and 24 longitudinal lattices. The number of azimuth locations per blade revolution is 60; i.e., the azimuth angle of each step is 6° (see Fig. 1(c)).

The comparison of low speed shaft torque between simulations and the NREL Phase-VI experiment is shown in Fig. 2. Fig. 3 show C_n and C_t at 7 m/s of wind speed. The results calculated by the proposed method (considering the tower) are in good agreement with the experimental results. However there is no significant disparity whether the tower is included or not, because the blade-tower interaction in the upwind configuration occurs in an instant, and represents a very small portion of the averaging or integrating value.

The time history of M_{fb} of the NREL Phase VI S sequence [16] was compared with the results of the proposed method for head-on flow of 5, 8, and 10 m/s (see Figs. 4) and 5°, 10°, and 20° of yaw error at 5 m/s (see Figs. 5). The difference between M_{fb} of simulation and M_{fb} of prediction at180° of azimuth angle is about 20 Nm, and the phase difference is 4° in all yaw error cases. The deficits of M_{fb} at each wind

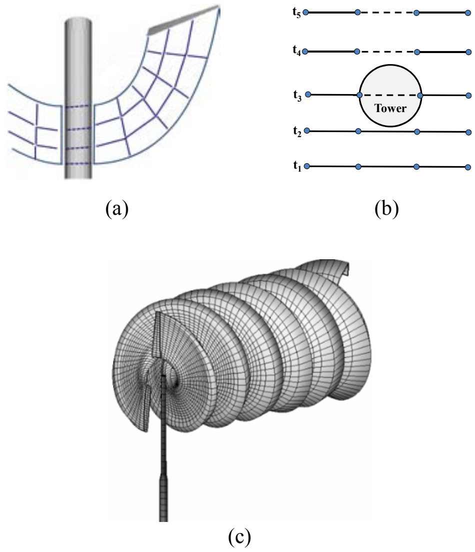

Fig. 1. Schematic view of blades and tower vortex lattices and wake panels for simulation: (a) front view of wake collision with tower; (b) top view of collision with tower; (c) whole panel system of wakes, blades and tower: spanwise-20 panels, chord wise-2 panels, 60 steps per 1 revolution.

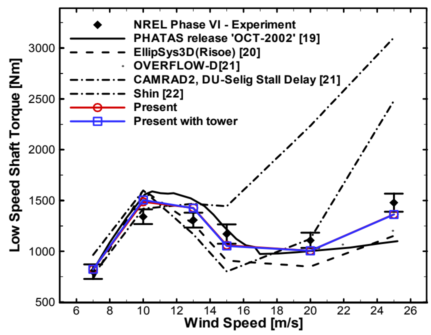

Fig. 2. Low speed shaft torque in various wind speed: OVERFLOW-D and EllipSys3D are CFD solver. PHATAS's, Shin's and CAMRAD2's results are based on potential flow.

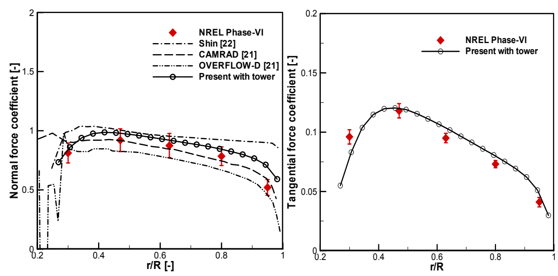

(a) C_n (b) C_t

Fig. 3. C_n and C_t at 7 m/s, head-on flow: OVERFLOW-D and is CFD solver. Shin's and CAMRAD2's results are based on potential flow.

speed and yaw error were accurately predicted using the proposed method. Given these interpretations of our results, it is highly probable that this method can be used for qualitative parametric study.

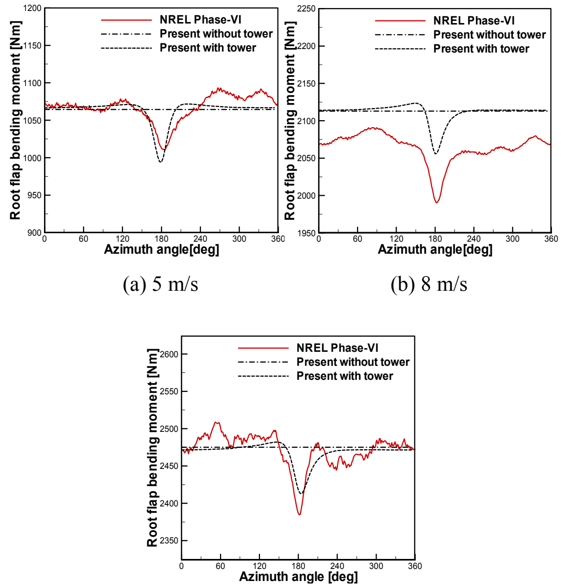

(a) 5 m/s (b) 8 m/s

(c) 10 m/s

Fig. 4. Comparison of prediction and experiment of M_{fb} at various wind speed in head on flow condition.

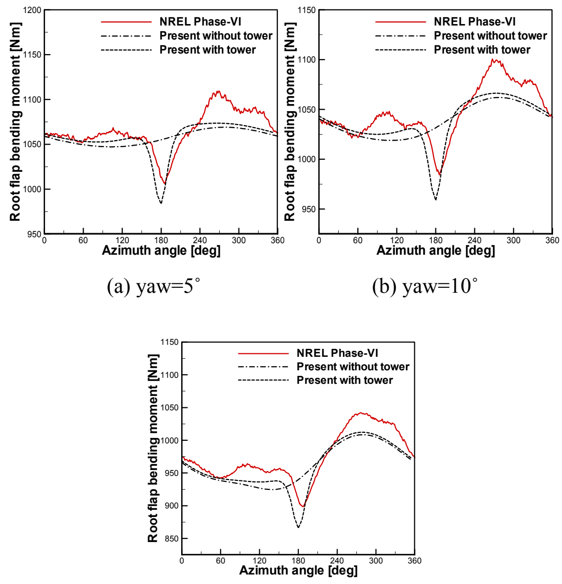

(a) yaw=5˚ (b) yaw=10˚

(c) yaw=20˚

Fig. 5. Comparison of prediction and experiment of M_{fb} at various yaw errors in 5 m/s: phase difference between predictions and experiments is 4˚.

4. Numerical simulations

4.1 Head-on flow

The effective angle of attack distribution at a wind speed of 5 m/s is shown in Fig. 6. Fig. 7 represents the normalized in coming velocity of in-plane and out-of-plane velocities for r/R=0.9. As seen in Figs. 6 and 7, the blockage effect of the tower reduced the out-of-plane velocity, and then the effective angle of attack. In contrast, when the blade section approaches the tower, the incoming in-plane velocity is increased, and when the blade section moves away from the tower, the incoming in-plane velocity is decreased. These phenomenon change the aerodynamic loading at each blade section.

Table 1. Phase VI turbine machine parameters.

Rotor diameter	10.058 m	Rated power	19.8 kW
Hub height	12.192 m	Tilt	0˚
Rotational Speed	71.63 RPM	Cone	0˚,3.4˚,18˚
Cut-in speed	6 m/s	Tower diameter	0.6096 m(base), 0.4064 m(top)
Power regulation	Stall	Tower clearance	1.401 m

Table 2. Chord and Twist distribution of the NREL Phase VI blade.

Radial distance(m)	r/R(-)	Chord(m)	Twist(˚)
1.257	0.250	0.737	20.040
1.952	0.388	0.666	7.979
2.343	0.466	0.627	4.715
2.867	0.570	0.574	2.083
3.185	0.633	0.542	1.115
3.476	0.691	0.512	0.494
3.781	0.752	0.482	-0.015
4.023	0.800	0.457	-0.381
4.391	0.873	0.420	-0.920
4.696	0.934	0.389	-1.352
5.000	0.994	0.358	-1.775

Table 3. Normal force coefficient in head on flow condition.

Wind speed [m/s]	r/R(-)	C_n average	ΔC_n/mean C_n
5	0.30	0.360	0.172
	0.50	0.540	0.100
	0.75	0.504	0.074
	0.95	0.435	0.062
15	0.30	1.775	0.026
	0.50	1.366	0.022
	0.75	0.918	0.0052
	0.95	0.875	0.077
20	0.30	2.035	0.029
	0.50	1.540	0.024
	0.75	0.875	0.023
	0.95	0.719	0.0053

The change in the angle of attack by the blade-tower interaction at the blade root region was greater than that on the outer part (see Fig. 8) because the blade-tower interaction of the blade tip region is limited to a small fraction of the blade cycle. The standard deviation of the effective angle of attack increased as the wind speed increased because the wind speed deficit by the tower increased with wind speed. The normal forces acting on the blade at each section (r/R=30% and 75%) are plotted in Fig. 9. In opposition to the change in the effective angle of attack, the change in C_n decreased as the wind speed increased; this is because when the wind speed was greater than 15 m/s, the flow was partially or totally separated along the blade. In this case, the lift and drag did not change as much as the change in angle of attack. As seen in Fig. 9, Fig. 10 and Table 3 show that the response of the blade-tower in-

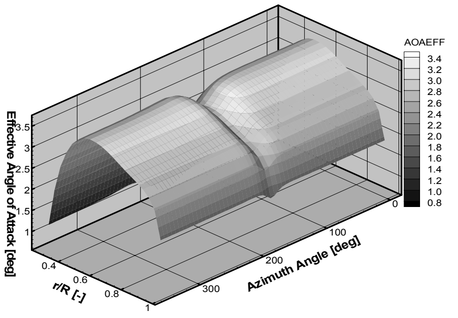

Fig. 6. Time history of effective angles of attack distribution at 5 m/s in head on flow: tower is in 180˚.

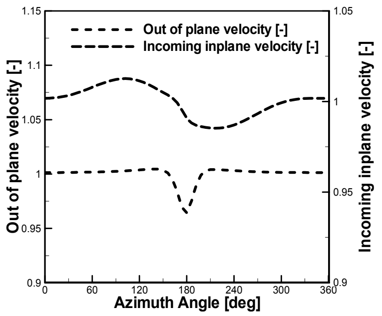

Fig. 7. Normalized velocity of wind direction and incoming in plane in r/R=0.9.

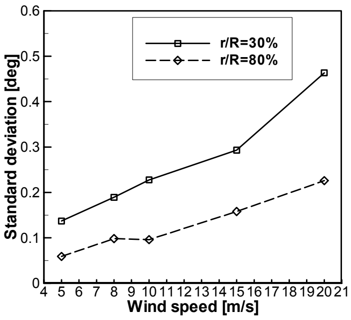

Fig. 8. Standard deviation of effective angle of attack in head on flow condition.

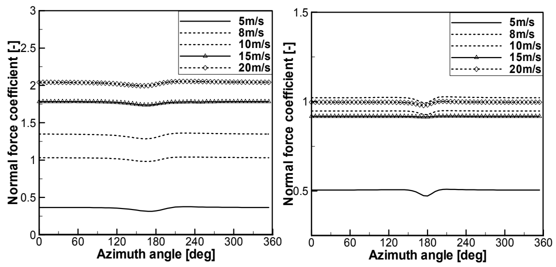

(a) r/R=30% (b) r/R=75%

Fig. 9. C_n versus azimuth angle at various wind speeds in head on flow condition.

teraction was small on the outer part of the blade.

With regard to fatigue load, in downwind type the deviation of C_n and r/R=0.3 (see Ref. [14]); however, in the upwind type,

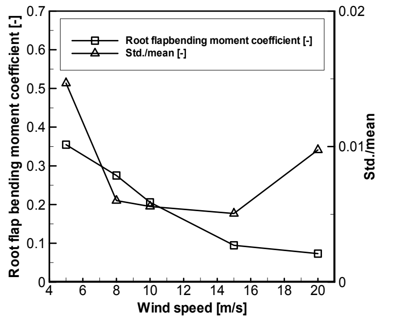

Fig. 10. C_{Mfb} and normalized σ_{Mfb} versus wind speed in head on flow condition.

the deviation was about 0.057 at 10 m/s and r/R=0.3 (Fig. 9(a)). Although the effect of blade-tower interaction of the upwind type was much smaller than that of the downwind type, it can be seen in Ref. [5] that the tower contributed 10% to the total fatigue loading. As seen in Table 3, at 5 m/s and for a fully-attached flow condition, the change in the normal force coefficient (C_n max- C_n min) normalized to the average value for all spanwise sections was approximately 10%. That is about 3.2% at 15 m/s for a partially separated flow, and about 2% at 20 m/s for a fully stalled condition. Fig. 10 describes C_{Mfb} and σ_{Mfb} normalized to the average value. The effect of blade-tower interaction for a specific wind speed condition cannot be compared to that of other wind speed conditions because M_{fb} increased with wind speed. However, σ_{Mfb} normalized to the mean value decreased as the wind speed increased up to 15 m/s. At wind speeds of 10 m/s and 15 m/s, the flow condition partially separated and the condition at 20 m/s was fully separated. In the partially separated condition, lift and drag did not change dramatically with the angle of attack, but at 20 m/s, the drag increased.

4.2 Yawed flow

The phenomenon of yaw error is similar to a helicopter forward flight. The advancing side of a helicopter in forward flight is around 180˚ of azimuth angle, and the region around an azimuth angle of 0˚ is similar to the retreating side of a helicopter in forward flight. In the blade root region, the angle of attack changes more significantly compared to other regions (see Fig. 11) because near that region, the wind speed is greater than the rotational component of the vector sum of the blade section velocity. As seen in Fig. 12 and Table 4, at the blade root region, the blade-tower interaction is larger than the other region. The change of C_n (C_n max- C_n min) by the blade-tower interaction (the last column of Table 4) is about 8.7% greater than the rotational component of the vector sum of the blade section velocity. As seen in Fig. 12 and Table 4, at the blade root region, the blade-tower interaction is larger than the other region. The change of C_n (C_n max- C_n min) by the blade-tower interaction (the last column of Table 4) is about 8.7% of the mean C_n at 5˚ of yaw error, about 8.5% of the mean C_n at 10˚ of yaw error, and about 8% of the mean C_n at 20˚ of yaw

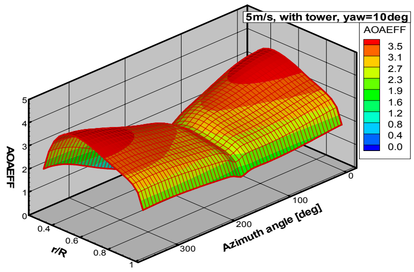

(a) With tower

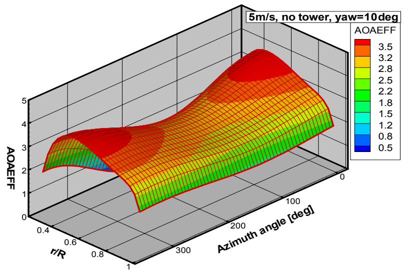

(b) Without tower

Fig. 11. Time history of effective angles of attack distribution at V_∞=5 m/s and yaw=10˚.

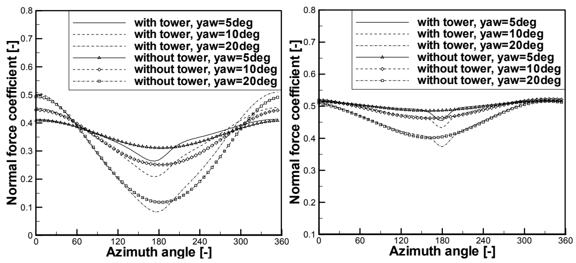

(a) r/R=30% (b) r/R=75%

Fig. 12. C_n versus azimuth angle in various yaw errors at V_∞=5 m/s.

error for all spanwise sections for a wind speed of 5 m/s. The difference between C_n max and C_n min by the blade-tower interaction decreases as yaw error increases.

The differences in the normalized σ_{Mfb} with the blade-tower interaction and without the blade-tower interaction decrease with yaw error because of the decline of wind speed perpendicular to the rotor plane (Fig. 13).

4.3 Wind shear

The wind velocity at the height of the blade section was deduced from a power law function recommended by IEC (International Electrotechnical Commission) 61400-1 as follows:

$$\frac{Vz}{Vz_r} = \left(\frac{z}{z_r}\right)^{\gamma} \tag{8}$$

where Vz is the wind speed at height z, Vz_r is the reference wind speed at height z_r, and γ is the power law exponent. z_r is

Table 4. Normal force coefficient in yawed flow condition at 5 m/s.

Yaw error (deg)	r/R(-)	C_n average with tower(1)	C_n average without tower(2)	ΔC_n with tower/(1)-ΔC_n without tower/(2)
5	0.30	0.358	0.359	0.145
	0.50	0.537	0.538	0.087
	0.75	0.501	0.527	0.065
	0.95	0.433	0.483	0.051
10	0.30	0.348	0.346	0.144
	0.50	0.527	0.501	0.088
	0.75	0.493	0.493	0.065
	0.95	0.426	0.460	0.046
20	0.30	0.305	0.296	0.128
	0.50	0.484	0.432	0.093
	0.75	0.460	0.425	0.065
	0.95	0.400	0.399	0.037

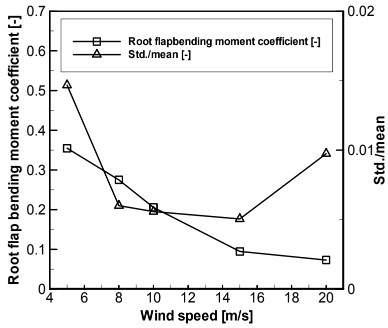

Fig. 13. C_{Mfb} and normalized σ_{Mfb} versus yaw errors at V_∞=5 m/s.

the hub height, and the reference wind speed is 5 m/s. Wind-shear exponent γ is determined in two different ways. First, the wind shear exponent is derived from the site terrain roughness length [23] based on the wind profile in the turbulent boundary layer of a neutral atmosphere. Second, we determine the wind shear exponent by atmospheric stability based on the net heat flux to the ground. The atmospheric states and wind shear exponents are categorized according to six steps [24]. We used wind shear exponents of 0.09, 0.20, and 0.41. The wind shear exponent of 0.09 represents a very unstable atmospheric state, 0.20 describes a neutral state, and 0.41 describes a very stable state.

The difference in C_n from azimuth˚ 0˚ to 180˚ increased with the wind shear exponent because the reference position was determined at the hub height, and the wind speed was the same for all wind shear exponents at the hub height at azimuths of 90˚ and 270˚. The blade-tower interaction was relatively stronger at the root position (see Fig. 14(a), Table 5). In contrast to the yaw error cases, the changes and the time history pattern of C_n were almost the same for each wind shear exponent regardless of the spanwise position. The change of C_n (C_n max- C_n min) normalized to the mean C_n of the blade-tower interaction (the last column of Table 5) slightly decreased at each section as the wind shear exponent increased.

The in-plane velocity did not change at each section for all azimuths; however, the out-of-plane velocity changed by wind

Table 5. Normal force coefficient in wind shear flow condition at 5 m/s.

Shear γ	r/R(-)	C_n average		ΔC_n with tower/(1)-ΔC_n without tower/(2)
		with tower(1)	without tower(2)	
0.09	0.30	0.360	0.365	0.141
	0.50	0.540	0.542	0.083
	0.75	0.504	0.503	0.060
	0.95	0.434	0.432	0.052
0.21	0.30	0.360	0.365	0.143
	0.50	0.540	0.542	0.083
	0.75	0.503	0.503	0.060
	0.95	0.434	0.431	0.052
0.44	0.30	0.361	0.366	0.143
	0.50	0.541	0.542	0.083
	0.75	0.503	0.503	0.059
	0.95	0.435	0.432	0.050

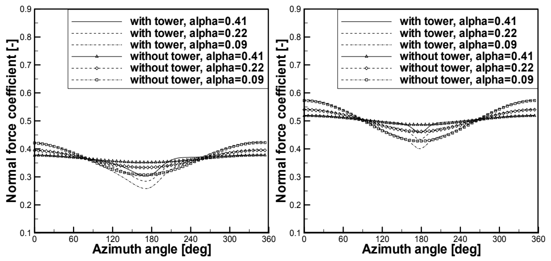

(a) r/R=30% (b) r/R=75%

Fig. 14. C_n versus azimuth angle in various wind shear exponents at V_∞= 5 m/s.

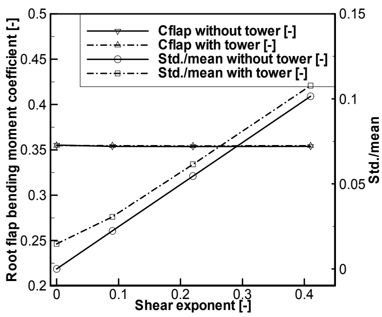

Fig. 15. C_{Mfb} and normalized σ_{Mfb} versus wind shear exponents at V_∞= 5 m/s.

shear according to height. This is different than the yaw error case.

As seen in Fig. 15, C_{Mfb} by the shear exponent and tower are almost constant. As previously mentioned, the reason is that the reference position is the hub height, and the increase in wind speed as the blade is over the hub height compensates the deficit of wind speed when the blade is in a down position from 90˚ of azimuth to 270˚ of azimuth. The normalized σ_{Mfb} sharply increased with wind shear. The normalized σ_{Mfb} of the very stable state increased by a factor of about three compared to the normalized σ_{Mfb} of the unstable state because of the large deviation in wind speed due to the very stable atmospheric state. The difference between the normalized σ_{Mfb} with the tower and without the tower decreased slightly as the wind shear exponent increased.

4.4 Tower variations

To study blade-tower interactions with respect to tower diameter and tower clearance, simulations representing 50%, 100%, 200%, and 300% (below 0.5r, r, 2r, and 3r cases) of the baseline tower radius were performed. Note that tower clearances for all tower radius variations were the same. Tower clearance cases, tower approaches to rotating plane by one times the tower diameter (below -1d case) from the baseline position and tower moves away from the base line position by one and two (below +1d and +2d cases) times the tower diameter, also were calculated.

As shown in Figs. 16-18, the 3r case had the greatest influence on blade tower interaction. The blade-tower interaction effect of the 2r case is greater than that of the -1d case. The azimuth angle range induced by tower interaction increased as the tower radius increased. C_{Mfb} were almost constant with increasing tower radius, and the normalized σ_{Mfb} of the 0.5r case was about 1/4 of the baseline case.

As the tower radius reached twice the baseline tower radius, the normalized standard deviation increased to 3.5 times that of the baseline case. The normalized standard deviation of the 3r case increased to 7.8 times that of the baseline case (see Fig. 18(a)).

C_{Mfb} was not changed by various tower clearances. In the -1d case, the normalized σ_{Mfb} increased 1.7 times compared to the normalized case. When the tower clearance increased twofold compared to the baseline tower diameter, the normalized standard deviation decreased to two-thirds of the baseline case. The normalized standard deviation of the -3d case was about 50% of the baseline case. In this study, the influence of blade-tower interaction was higher on the aerodynamic loading of tower radius variations than on the aerodynamic loading of tower clearance variations.

5. Discussion

The proposed numerical method accurately predicted the deficits of the root flap bending moment. We conclude that the proposed method is suitable for computing the blade-tower interaction. However, there is an additional argument that the main source of the fluctuations of the experimental data (that could not be found in the simulation results) is to be found elsewhere.

Turbulence intensity is generally a function of roughness. If roughness is constant and a deviation in wind speed increases with wind speed, then the stochastic loads on a rotor blade increase. Therefore, it may be the case that for relatively high winds (i.e., over 8 m/s--it is hard to decide what high wind is, and this issue is beyond the scope of our study) the blade-tower interaction effect on the total fatigue load decreases. Moreover, the fatigue load increases due to stall at high wind speeds in a stall control wind turbine, so the blade-tower interaction maybe not play an important role in total aerodynamic loading at high wind speeds. In other words, because the standard deviation of wind speed is low at low wind speeds, the

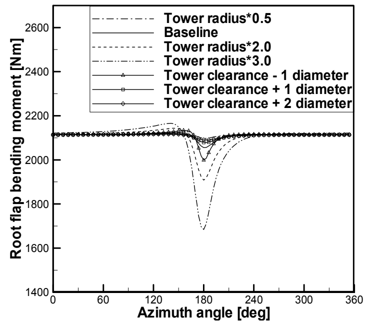

Fig. 16. M_{fb} in various tower condition at V_∞=8 m/s.

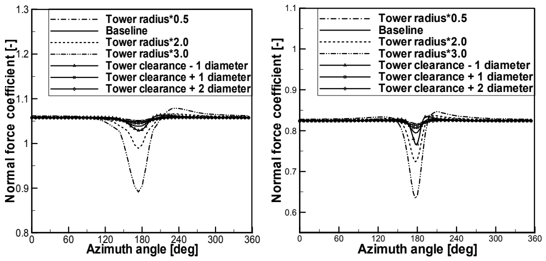

(a) r/R=50% (b) r/R=95%

Fig. 17. C_n versus azimuth angle in various tower conditions at V_∞=8 m/s.

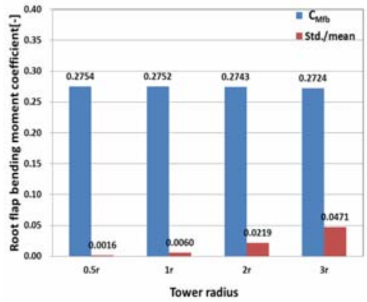

(a) Tower radius variations

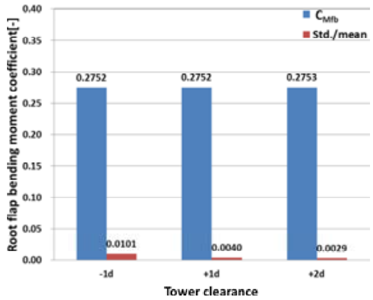

(b) Tower clearance variations

Fig. 18. C_{Mfb} and normalized σ_{Mfb} versus tower conditions at V_∞= 8 m/s.

blade-tower interaction at low wind speeds can be more important compared to blade-tower interaction at high winds.

As the wind shear exponent increases, the change of wind according to height increases, and the stochastic fatigue load increases. As a result, the blade-tower interaction effect on blade fatigue load may be insignificant as the wind shear exponent increases. However, an offshore atmosphere may have weaker turbulence intensity in the air. Therefore, the blade-tower interaction may have some effect on fatigue load.

6. Discussion

We attempted to validate the proposed numerical solver, and we examined the interaction between a tower and a rotor blade in an upwind-type horizontal axis wind turbine system. Moreover, we parametrically examined various wind conditions (uniform flow, wind shear, and yaw error) and tower conditions (various radius and tip clearance cases). To validate the proposed numerical method, experimental results from the NREL Phase-VI rotor sequence S were compared with the results from the numerical method. The simulation results were in good agreement with the experimental results. The upwind-type HAWT blade-tower interaction is a block gage effect that reduces inflow wind speed on the rotor plane, which then changes the angles of attack and the aerodynamic loading. The response of the blade-tower interaction is relatively small on the outer part of the blade because of the small fraction of the blade rotation. The root region of the rotor has a larger azimuth range of the blade-tower interaction and a greater change in aerodynamic loading compared to the tip region. At 5 m/s (a fully attached flow condition), the change in the normal force coefficient (C_n max- C_n min) is approximately 10% of the C_n average for all spanwise sections. That is about 2% at 20 m/s for a fully stalled condition. We found that the tower interaction decreased as the yaw error and wind shear exponent increased. Note that the reference height is the hub position for the wind shear calculation. In light of the fatigue load, we note that the blade-tower interaction did not significantly affect the total fatigue load of the rotor blade at relatively high winds and more stable atmospheric conditions because as wind speed and wind shear exponent increased, the stochastic fatigue load increased due to the turbulence of the atmosphere. (It is hard to determine the boundary at which the blade-tower interaction becomes quantitatively important, and this is beyond the scope of the study.) The offshore atmosphere has a relatively weak atmospheric turbulence condition; therefore, it is possible that the blade-tower interaction has some degree of effect on rotor blade fatigue load. Our results show that the blade-tower interaction due to tower radius variations was higher than that by tower clearance variations. To reduce the blade-tower interaction, it can be more effective to decrease the tower radius.

We have described a limited parametric examination of the blade-tower interaction. Further study is required concerning the quantitative blade-tower interaction with respect to turbine scale, wind turbine size, pitch and stall control, and atmospheric turbulence.

Acknowledgment

This work was supported by the Human Resources Development of the Korea Institute of Energy Technology Evaluation and Planning (KETEP) grant funded by the Korea government Ministry of Knowledge Economy (No. 20094020100060) and by the New and Renewable Energy Program of the Korea Institute of Energy Technology Evaluation and Planning (KETEP) grant funded by the Korea government Ministry of Knowledge Economy (No.20104010100490).

Nomenclature

C_d : Sectional drag coefficient (dimensionless)
C_{Mfb} : Root flap bending moment coefficient ($M_{fb} / (0.5\rho V_\infty^2 \pi R^2 0.5R)$, dimensionless)
C_l : Sectional lift coefficient (dimensionless)
C_n : Sectional normal force coefficient (dimensionless)
C_t : Sectional tangential force coefficient (dimensionless)
D : Drag force (N)
$\boldsymbol{F}$: Lift difference between UVLM and table look-up (N)
L : Lift force (N)
M_{fb} : Root flap bending moment (Nm)
$\boldsymbol{n}$: Normal vector of body panel (dimensionless)
R : Rotor radius (m)
$\boldsymbol{r}$: Radial position vector to rotating origin (m)
t : Time (s)
V : Onset velocity of strip (m s^{-1})
$\boldsymbol{V_B}$: Total velocity of body (m s^{-1})
$\boldsymbol{V_\infty}$: Free stream velocity (m s^{-1})
Vz : Wind speed at height z

Greek letters

Γ : Bound vortex strength (m^2 s^{-1})
$\Gamma_{T.E}$: Trailing edge panel circulation (m^2 s^{-1})
Γ_W : Wake panel circulation (m^2 s^{-1})
Φ^* : Total potential
$\boldsymbol{\Omega}$: Rotor velocity (rad s^{-1})
α : Effective angle of attack (degree, °)
γ : Power law exponent of wind shear (dimensionless)
ρ : Air density (kg m^{-3})
σ_{Mfb} : Standard deviation of root flap bending moment (Nm)

References

[1] UPWIND Project. http://www.upwind.eu, accessed on: 3 July 2010.
[2] R. Harrison, E. Hau and H. Snel, *Large wind turbine: Design and Economics*, John Wiley & Sons. Ltd, West Sussex, England (2000) 1-26.
[3] EWEA, *WIND ENERGY – THE FACTS PART I: TECHNOLOGY*, European Wind Energy Association (2009) 72-79.
[4] M. O. L. Hansen, J. N. Sørensen, S. Voutsinas, N. Sørensen and H. A. Madsen, State of the art in wind turbine aerodynamics and aeroelasticity, *Progress in Aerospace Sciences,* 42 (2006) 285-330.
[5] C. Bak, H. Aagaard Madsen and J. Johansen, Influence from blade-tower interaction on fatigue loads and dynamics, *EWEC '01 Proceedings* (2001) 394-397.
[6] J. M. R Graham, C. J. Brown and G. Giannakidis, Aerodynamic interaction between wind-turbine rotor blades and the tower, *EVEC '01 Proceedings* (2001) 359-361.
[7] J. J. Chattot, Extension of a helicoidal vortex model to account for blade flexibility and tower interference, *J. Solar Energy Eng.,* 128 (2006) 455-460.
[8] H. G. Kim, S. M. Lee and S. G. Lee, Numerical analysis on the aerodynamics of HAWTs using nonlinear vortex strength correction. *Current Appl. Phys.,* 10 (2010) S311-S315.
[9] L. Prandtl and O. G. Tietjens, *Applied hydro-and aeromechanics*, *DOVER*, New York, USA (1934).
[10] A. van Garrel, *Development of wind turbine aerodynamics simulation module.* ECN-C-03-079, Aug. (2003).
[11] W. F. Philips WF and D. O. Snyder, Modern adaptation of Prandtl's classic lifting-line theory, *J. Aircraft,* 37 (4) (2000) 662-670.
[12] NWTC Design Codes (AirfoilPrep by Dr. Craig Hansen), *http://wind.nrel.gov/designcodes/preprocessors/airfoilprep/.* Last modified 16-January-2007, accessed on: 16-January-2007.
[13] W. H. Press, S. A. Teukolsky, W. T. Vetterling and B. P. Flannery, *Numerical recipes in fortran: the art of scientific computing, 2nd edition*, Cambridge University Press, Cambridge, England (1992) 372-386.
[14] F. Zahle, N. N. Sørensen and J. Johansen, Wind turbine rotor-tower interaction using an incompressible overset grid method, *Wind Energy,* 12 (6) (2009) 594-619.
[15] G. V. Parkinson and T. Jandali, A wake source model for bluff body potential flow, *J. Fluid Mech.,* 40 (3) (1970) 577-594.
[16] M. M. Hand, D. A. Simms, L. J. Fingersh, D. W. Jager, J. R. Cotrell, S. Schreck and S. M. Larwood, *Unsteady aerodynamics experiment phase VI: Wind tunnel test configurations and available data campaigns*, NREL/TP-500-29955 (2001).
[17] D. Simms, S. Schreck, M. Hand, L. Fingersh, J. Cotrell, K. Pierce and M. Robinson, *Plans for testing the NREL unsteady aerodynamics experiment 10-m diameter HAWT in the NASA Ames wind tunnel*, NREL/TP-500-27599 (1999).
[18] D. Simms, S. Schreck, M. Hand and L. Fingersh, *Unsteady aerodynamics experiment in the NASA-Ames wind tunnel: comparison of predictions to measurements*, NREL/TP-500-29494 (2001).
[19] C. Lindenburg, *Investigation into rotor blade aerodynamics, analysis of the stationary measurements on the UAE phase-VI rotor in the NASA-Ames wind tunnel,* ECN-C-03-025 (2003).
[20] N. N. Sørensen, J. A. Michelsen and S. Schreck, Navier-Stokes predictions of the NREL Phase-IV rotor in the NASA Ames 80-by-120 wind tunnel, *AIAA Paper No. 2002-0031, ASME Wind Energy Symposium* (2002) 94-105.
[21] E. P. N Duque, M. D. Burklund and W. Johnson, Navier-Stokes and comprehensive analysis performance predictions

of the NREL phase VI experiment, *AIAA Paper No. 2003-0355, ASME Wind Energy Symposium* (2003) 1-19.
[22] Hyungki Shin, *Numerical and experimental analysis of performance, aerodynamic load and noise on HAWT blade.* Ph.D. Dissertation, Dept. of Aerospace Engineering, Seoul National University (2005).
[23] A. P. van Ulden and J. Wieringa, Atmospheric boundary-layer research at Cabauw, *Boundray-layer Mereorology,* 78 (1996) 39-69.
[24] TA-Luft, Erste Allgemeine Verwaltungsvorschrift zum Boundes-Immissionsschurzgesetz-Technische Anleitung zur Reinhaltung der Luft (First General Directive to the Federal Immission Protection Act-Technical Guideline for Clean Air in German), (1986).

Hogeon Kim is a Ph.D. candidate in Mechanical and Aerospace Engineering at Seoul National University. He received his B.S degree in Mechanical Engineering from Ajou University. His main research fields cover rotating machine aeroacoustics and aerodynamics. Especially, his research interests are the aerodynamic analysis and aerodynamic noise prediction of wind turbine systems.

Seungmin Lee is a Ph.D. candidate in Mechanical and Aerospace Engineering at Seoul National University. He received his B.S. degree in Mechanical and Aerospace Engineering from Seoul National University. His research interests are in the area of aerodynamics and acoustics of rotating machines.

Soogab Lee is a professor at the department of mechanical and aerospace engineering in Seoul National University. He received his Ph.D. degree in aeronautics and astronautics from Stanford University in 1992. He worked as an research scientist at NASA Ames Research Center from 1992 to 1995. His research interests are in the area of aerodynamics and acoustics of rotating machines including wind turbine systems.